

# LONG-DISTANCE INTERFEROMETRY WITH AN He-Ne LASER\*

F. T. Arecchi and A. Sona

*Laboratori Centro Informazioni Studi Esperienze, Milan, Italy*

*Interference fringes have been observed up to an optical path difference of 120 m (mirror separation 60 m) without a substantial loss of visibility. Laser output is split by a beam-splitter onto a Michelson interferometer through a telescope system which reduces the angular spread.*

*By changing the path difference continuously, in the first experiments the fringe visibility was subjected to a periodical change, going down to zero every time the path difference was an odd multiple of the cavity length. This is due to interference between different axial modes. To avoid this effect we have made both a transverse and an axial selection. The isolation of a TEM<sub>00</sub> pattern is accomplished by adjusting two movable diaphragms near the mirror. The selection of a single axial mode is done with an external plane mirror which acts as a second Fabry-Perot. This technique does not reduce the output power, as occurs when a near-threshold operation is used to isolate a single mode. On the contrary a power increase is observed in the useful mode.*

*An electronic system for measuring and analyzing experimental results is described and limitations on circuit bandwidth, observation time and precision are related to fluctuations within the interferometer system and associated circuitry.*

## 1. INTRODUCTION

We report a long-distance interferometry experiment where the source is a He-Ne laser working at the 6328 Å transition in single mode operation.

Interference fringes have been observed up to an optical path difference of 120 m (mirror separation 60 m) without a substantial loss of visibility.<sup>1</sup>

An experiment of this kind had already been performed with an infrared laser over a 9 m path difference<sup>2</sup> and a 100 m interference experiment with a visible gas laser has recently been reported.<sup>3</sup>

Three characteristic times can be associated with the laser interferometer:

1. The coherence time (in the classical sense) which limits the transit time between the Michelson mirrors. Our experiments show that a transit time of the order of  $10^{-6}$  sec is possible.

2. A time of the order of  $10^{-3} - 10^{-1}$  sec which characterizes the elastic fluctuations of the interferometer frame and the acoustical and thermal fluctuations of the traversed medium, and which contributes a limitation on the observation time  $T$  in order to reach a given precision.

\*Work done with the financial support of the Consiglio Nazionale delle Ricerche.

---

Presented at the Symposium on Quasi-Optics,  
Polytechnic Institute of Brooklyn, June 8, 9, 10, 1964

3. A time of the order of minutes which characterizes the thermal drifts of the frame and the stability of the laser itself.<sup>4</sup>

Much work has to be done to improve the times 2 and 3 above. For the present experiments, an electronic observation system has been designed which optimizes the available output despite noise and fluctuation considerations.

## 2. EXPERIMENTAL APPARATUS AND RESULTS

The experimental setup is shown in Fig. 1. We have used a confocal cavity of 2 m length. The second surface of the mirrors is corrected in order to have a plane wave output. The gas discharge is fed by a current stabilized dc supply in order to avoid any fluctuation or 50 cps line ripple.

The laser output is split by a beamsplitter  $M_1$  onto a Michelson interferometer through a telescope system which reduces angular spread. The two Michelson mirrors A and B are made as two cat's-eye systems for easier alignment. This allows one to span a long distance on a conventional optical bench without re-adjusting the system.

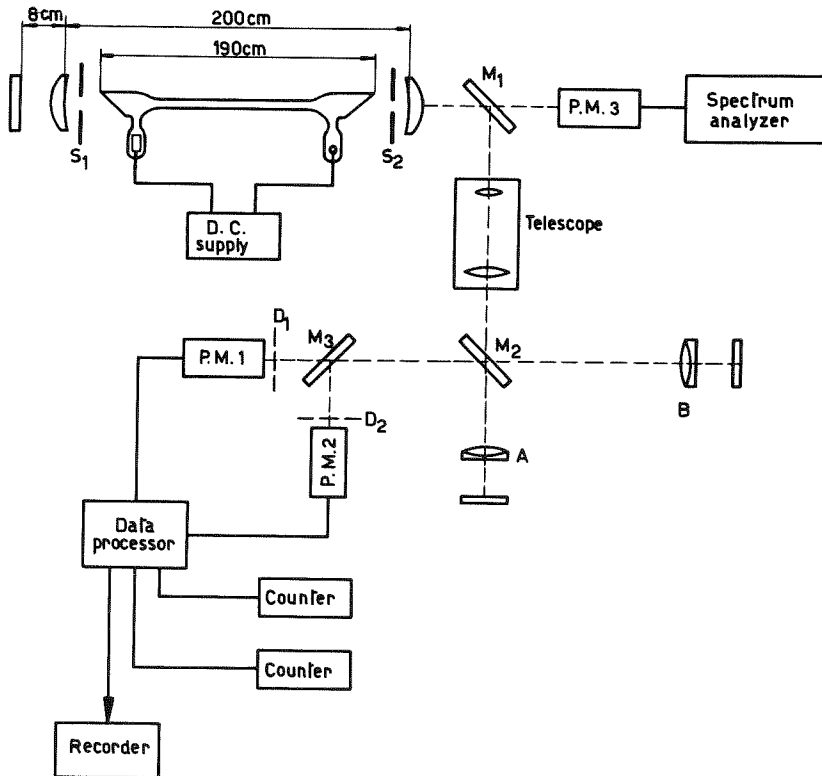


Fig. 1. Experimental setup.

In the first experiments, by continuously changing the path difference, the fringe visibility was subjected to a periodical change, going down to zero every time the path difference was an odd multiple of the cavity length. This is due to interference between different axial modes, as has been already pointed out in Ref. 2. To avoid this effect, we have made both a transverse and an axial mode selection. The isolation of a  $TEM_{00}$  pattern is accomplished by adjusting two movable diaphragms  $S_1, S_2$  near the mirrors. The selection of a single axial mode is done with an external plane mirror (99% reflectivity), which acts as a second Fabry-Perot.<sup>5,6</sup> The result was checked by observing the beat frequencies on a spectrum analyser. The position and alignment of this external mirror were adjusted so that the strengths of the first four beats (75, 150, 225 and 300 Mc/sec., respectively) were reduced by more than 20 db. This technique does not reduce the output power, as occurs when a near-threshold operation is used to isolate a single mode. On the contrary, a power increase is observed in the useful mode.

Figure 2(a) shows the fringe pattern observed with this technique for a 6 m path difference. At this point, the visibility would have been very poor if observed without the second Fabry-Perot. Figure 2(b) shows the fringe pattern for a path difference of 120 m.

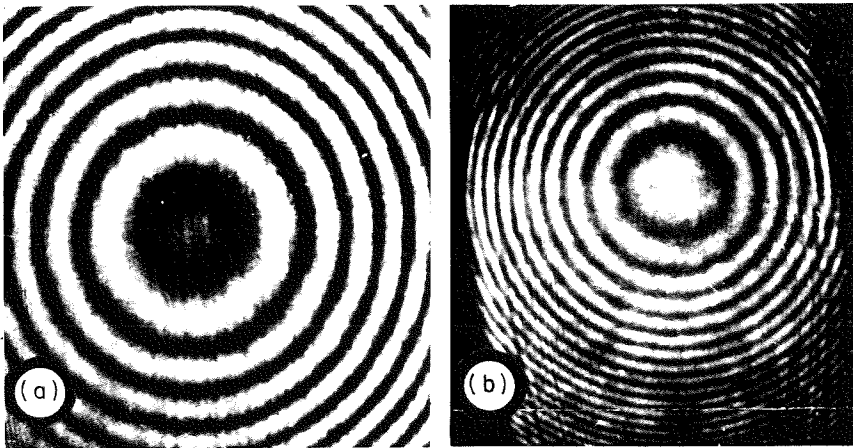


Fig. 2. (a) Interference fringes for a 6 m path difference (laser working with the second Fabry-Perot). Exposure time: 1/50 sec. (b) Interference fringes for a 120 m path difference. Exposure time: 1/100 sec.

Figure 3 shows the output from a phototube when the separation is 50 m. Line a gives the dark value; lines b and c give the intensities at the two Michelson arms; the fluctuating line d gives the shape of the fringes which changes due to random fluctuations of the optical length. The measured visibility is 86.2% and fits with the value calculated, taking into account the difference in amplitude between the channels and the ratio of the aperture width to the fringe spacing.\*

\*A visibility measurement through a densitometric analysis of a photographic plate is less straightforward, because one should take into account the nonlinear characteristic of the recording emulsion.

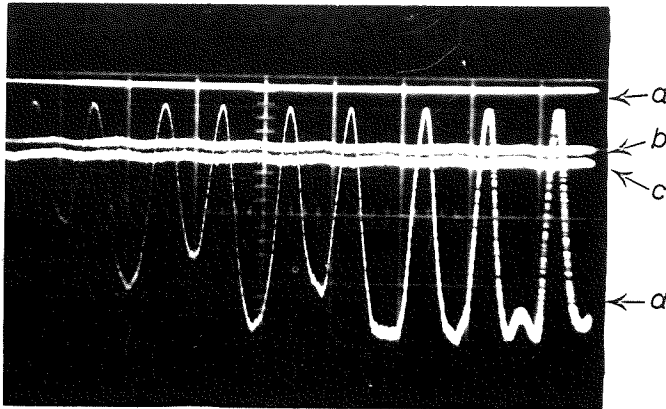


Fig. 3. Output from a phototube viewing the fringes, with a ratio slit-width/fringe spacing of about 0.4: (a) Zero line; (b) and (c) Intensities of the two separate beams; (d) Intensity of the interference pattern moving randomly. Time scale  $5 \times 10^{-3}$  sec/div.

The interference fringes are handled by an observation system designed for two different basic purposes: first, to check the stability in time of a fixed length up to 60 m with the resolution of an eighth of a wavelength; second, to allow an absolute measurement of a length between 0 and 60 m in number of eighths of wavelengths. The fringe image is projected on to a pair of photomultipliers P. M. 1 and P. M. 2 through annular slits in diaphragms  $D_1$  and  $D_2$  concentric to the fringe system and narrower than the fringe spacing. The two diaphragms select two regions of the fringe pattern phased about  $90^\circ$  apart in space in order to obtain information both on the number of fringes crossing the apertures and on the sense of the movement.

Since the fringe spacing changes as the path difference is changed, the phase difference between the outputs of the two photomultipliers cannot be kept constant with fixed diaphragms. An improved dephasing system, proposed by Peck and Obetz<sup>7</sup> is now being tested.

A two-channel electronic system, described elsewhere,<sup>8</sup> records the number of quarters of fringe passing across the diaphragm slits in one sense or the other. For fixed mirrors, the difference between the two counters yields the stability information. For moving mirrors, the number recorded in the counter and the sense of the movement yields the measurement of the scanned length with a resolution of  $\lambda/8$  and a maximum speed of  $10^5$  pulses/sec.

### 3. CIRCUIT DESIGN AND LOGIC OF THE OBSERVATION SYSTEM

The system for observing and analyzing the interferometer measurements provides storage and transmittal of experimental results in real time.

An electronic system extracts information on rate, direction and number of fringe pattern changes from the annular apertures in the diaphragms  $D_1$  and  $D_2$  in Fig. 1 which are illuminated by the interferometer output. The apertures are

concentrically related rings spaced approximately a quarter of a fringe apart within the fringe pattern area to provide electrical outputs from photomultipliers P. M. 1 and P. M. 2, which are in time quadrature to each other for any change in spacing or position of fringes in the interferometer pattern. The photocell outputs produce a Lissajous pattern on an oscilloscope when connected to its  $x$  and  $y$  terminals. A complete loop of the pattern corresponds to a full cycle of the fringe pattern and thus a change of path length of  $\lambda$ , or an effective relative shift of the mirrors of  $\lambda/2$ . The instantaneous position of the spot on the Lissajous circle is a function of the path difference, with period  $\lambda$ . The sense of movement of the spot corresponds to the sense of motion of the moving mirror.

The Lissajous pattern provides a two-dimensional representation of the signals applied to two trigger (discriminator) circuits connected in the same manner as the oscilloscope terminals.

The trigger circuit threshold levels are set to correspond with quadrants of the oscilloscope trace and thus change their state every time the trace crosses the threshold level (respectively,  $a - a$  for channel  $A$ , and  $b - b$  for channel  $B$ ). Let us call  $A$  and  $\bar{A}$  the "on" and "off" states of the discriminator  $A$ ;  $A'$  and  $\bar{A}'$  the transitions  $\bar{A} \rightarrow A$  and  $A \rightarrow \bar{A}$ ; and do the same with  $B$ . In Fig. 4, the two threshold lines cross the Lissajous pattern to form a set of eight parameters, four associated with stationary states and four with transitions. When the interferometer is in a stable position, the corresponding point will be in one of the four

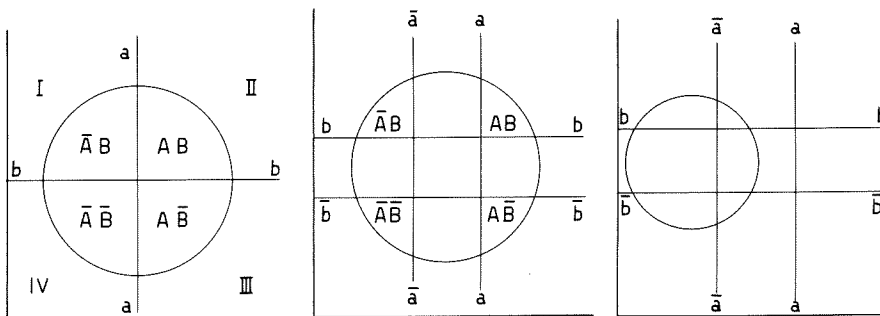


Fig. 4. Lissajous patterns built with the two phototube outputs.  $a - a$  and  $b - b$ : threshold lines of the discriminators.

quadrants, and can be located by two stationary parameters. When one mirror is moving with respect to the other, the motion is defined by the four crossings of the  $a - a$  and  $b - b$  diameters. These crossings are represented by the combination of the stationary state of one discriminator with the transition of the other. A full clockwise rotation of the spot, starting from the first quadrant, will give rise to the following series of events:

$$BA', \overline{AB'}, \overline{BA'}, \overline{AB'},$$

where each pair of letters denotes an "and" operation associated with the switching of quadrant, the first letter corresponding to the state of the discriminator which does not change, and the second to the transition of the other dis-

criminator. Similarly, a full counterclockwise rotation will give rise to the following events:

$$\overline{AB'}, \overline{BA'}, AB', \overline{BA'}$$

The first set of signals is logically summed onto an output  $X$  and the second onto an output  $Y$ , so a train of pulses is obtained from  $X$  and  $Y$ , for clockwise and counterclockwise rotations, respectively.

One can easily see that, for any fluctuation in the interferometer around a stable position, the oscillating Lissajous spot yields an equal number of counts at the two outputs  $X$  and  $Y$ . Therefore, the count difference is unaffected by

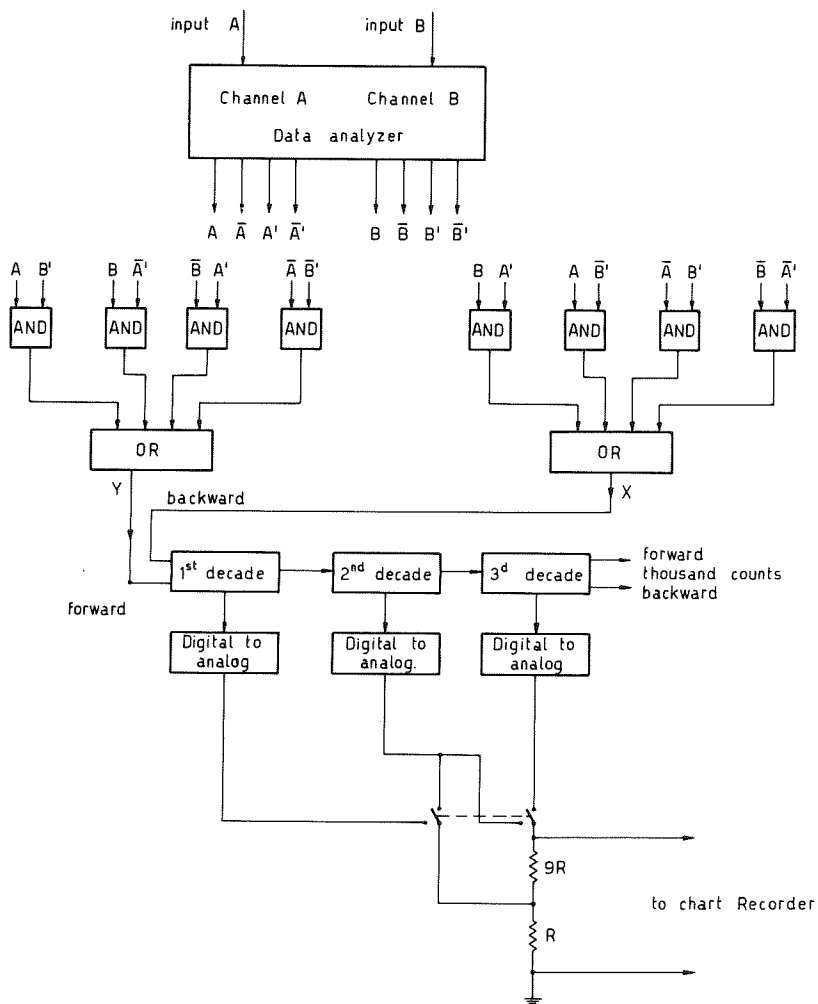


Fig. 5. Block diagram of the electronics.

spurious fluctuations with zero average, but changes by one every time there is an effective path difference of  $\lambda/4$ , corresponding to a  $\lambda/8$  shift in the moving mirror.

Hysteresis splits the switching levels introducing an imprecision smaller than the resolving power  $\lambda/8$  (Fig. 4(b)). Therefore the system is insensitive to hysteresis effects, unless a situation topologically equivalent to Fig. 4(c) occurs. Here one of the two discriminators can no longer switch and both  $X$  and  $Y$  outputs are zero, independently of the movement of the point on the Lissajous pattern.

These considerations are still valid when the two signals on the phototube are not equal in amplitude or out of quadrature, that is, when the Lissajous is no longer a circle, unless the topological equivalent of Fig. 4(c) occurs.

The block diagram of the circuitry is shown in Fig. 5.

A series of "and" and "or" circuits to handle the eight signals from the two discriminators, yields the following outputs:

$$X = \overline{AB'} + \overline{BA'} + \overline{AB'} + BA',$$

$$Y = \overline{AB'} + \overline{BA'} + AB' + B\overline{A'}.$$

The  $X$  and  $Y$  pulses are sent to a reversible decimal counter which yields the count difference as digital output or analog output to a chart recorder. A digital record of a stability and length measurement has been given in Ref. 1 over an observation time of about 50 sec, and with an integration time of 1 sec (see Ref. (1) for the technique used).

#### 4. CHARACTERISTIC TIMES OF AN INTERFEROMETRIC MEASUREMENT

A visibility measurement yields information on frequency stability (longitudinal coherence, in the classical sense) for time intervals of the order of the transit time of the light in the device. For example, with a working limit of 300 m, this time is around  $10^{-6}$  sec.

In addition, there is the contribution of the elastic fluctuations of the interferometer frame and the acoustical and thermal fluctuations of the crossed medium. As one can see from Fig. 3, the main contribution of these factors is a random movement of the fringes on a time scale of  $10^{-3}$ — $10^{-1}$  sec (depending on the working conditions). One can minimize these effects by putting the mirrors and the beam splitters of the interferometer on isolated pillars and sending the laser beam through evacuated pipes.

Actually, working in normal laboratory conditions on common optical benches, these effects, although present, give rise only to counts with zero average with the circuit logics of Sec. 3. Despite this zero average, this contributes to reducing the resolving power, as shown in the noise analysis of Sec. 5.

Finally on a long time scale ( $> 10$  sec), there are drifts due to the lack of stability of the laser itself and to thermal drifts of the interferometer arms. One can reduce the second effect with isolated pillars. The best data on laser stability thus far<sup>4</sup> gives a frequency resettability, over long periods of time, of one part in  $10^9$ .

When not using evacuated pipes, a much more severe limitation is present due to air turbulence. The fluctuations associated with the second characteristic time are due to the thermal motion of the air molecules in quiet air, as can be realized with some care in a laboratory. When the air is stirred up, a long distance measurement becomes almost meaningless. Professor Toraldo and his group are making an extensive analysis of these effects.<sup>9,10</sup>

## 5. NOISE CONSIDERATIONS AND LIMITS ON COUNTING SPEED AND OBSERVATION TIME.

Noise contributes a thickness to the Lissajous circle and two considerations put limits on it:

- a) The thickness of the circle should never be such as to make possible a random pattern within it, which acts as in Fig. 2(c).
- b) The thickness corresponding to the r.m.s. of the noise should not rise above the hysteresis level, in order to minimize noise triggered switching.

Otherwise the phototube noise can induce successive switching of the discriminator in a time shorter than the dead time of the following reversible counter. This dead time is  $\tau_2 \simeq 10\mu\text{s}$  as compared with  $\tau_1 \simeq 1\mu\text{s}$  of the system logic.

The two limitations can be summarized as follows:

$$i_s - \alpha i_n > i_H > \beta i_n \quad (1)$$

where  $i_H$  is the hysteresis current;  $i_n$  is the r.m.s. output noise from the photomultiplier tube;  $i_s$  is the signal current; and  $\alpha$  and  $\beta$  are shape factors defined in the following. These boundaries limit the region of possible values for  $i_H$ .

Some considerations are now given for  $\alpha$  and  $\beta$ .

### Calculation of $\beta$

The electronic circuitry employs the cascading of two different sets of circuits: the logics, with a bandwidth  $f_1$  and a corresponding dead time for counting  $\tau_1 = 1/(2f_1)$ , and the reversible counter with a dead time  $\tau_2 = 1/(2f_2)$ . The average rate of noise pulses can be measured on one channel for different values of  $i_H$  around  $I_0$ , and is given by:

$$f = f_1 e^{-\left(\frac{i_H}{2\sqrt{2}i_n}\right)^2} \quad (2)$$

The probability of more than one pulse on the same channel within the time is given by:

$$p \simeq f\tau_2 \quad (3)$$

because we shall design the  $i_H$  values such that  $f\tau_2 \ll 1$ .

The number of wrong counts per second due to noise is given by (4) and (5):\*

$$n = fp = f^2 \tau_2. \quad (4)$$

Furthermore any fluctuation in the optical path with zero average will give an extra number of counts per second  $F$ . The total number of wrong counts in the counter is then given by:

$$n = (f + F)^2 \tau_2. \quad (5)$$

As the wrong counts occur with the same probability in both senses, they give rise to a random walk in the position of the counter. After a time  $T$ , the position of the counter will be shifted from the correct one by a quantity which has zero average over a number of equally repeated measurements and a variance  $\sqrt{nT}$ . A consequent error arises in the measurement, because after a time  $T$  the position of the counter is affected by a standard deviation  $(f + F) \sqrt{\tau_2 T}$ . The ultimate precision of this measurement is given by  $F \sqrt{\tau_2 T}$ . The extra error  $f \sqrt{\tau_2 T}$  caused by the electronic circuitry can be minimized by setting the hysteresis at a level such that  $f < F$ . From (4), this condition corresponds to

$$\frac{i_H}{i_n} > 2\sqrt{2} \sqrt{\ln \frac{f_1}{F}} = \beta. \quad (6)$$

For instance, let us consider two different external conditions, with  $F_1 = 10^3/\text{sec}$  and  $F_2 = 10^2/\text{sec}$ , respectively. In our system,  $f_1 = 10^6/\text{sec}$ . In Fig. 6 we have shown upper and lower limitations  $i_s - \alpha i_n$  (a typical value is  $\alpha = 2$  as shown in Ref. 8) and  $\beta i_n$  vs.  $i_s$  for a stability measurement, taking into account that the noise current at the anode of a photomultiplier is given by:

$$i_n = \sqrt{2eGI_0 f_1 \frac{\delta}{\delta - 1}}$$

where  $f_1$  is the bandwidth of the electronics before the discriminators;  $\delta$  is the secondary multiplication factor of the dynodes;  $G$  is the phototube gain;  $I_0$  is the dc component of the phototube current at the threshold level of the discriminator; and the signal current  $i_s$  is related to the dc component  $I_0$  through the fringe visibility  $V$ :

$$V = \frac{I_{\max} - I_{\min}}{I_{\max} + I_{\min}} = \frac{i_s}{I_0}.$$

The set of parameters used is:

$$V = 1, \quad G = 10^6, \quad \delta = 4, \quad \alpha = 2, \quad \beta = 8,$$

and two values for  $f_1$ :  $10^6$  and  $10^5$  cps.

A limit to the longest observation time  $T$  arises from Eq. (5). If the noise

\*Furthermore, the average repetition rate should be reduced by a filling factor:

$$\eta = 4i_H/(2\pi i_s)$$

corresponding to the probability for the Lissajous spot of being in the hysteresis region. But for the sake of simplicity we shall assume  $\eta = 1$ , which is the least favorable condition.

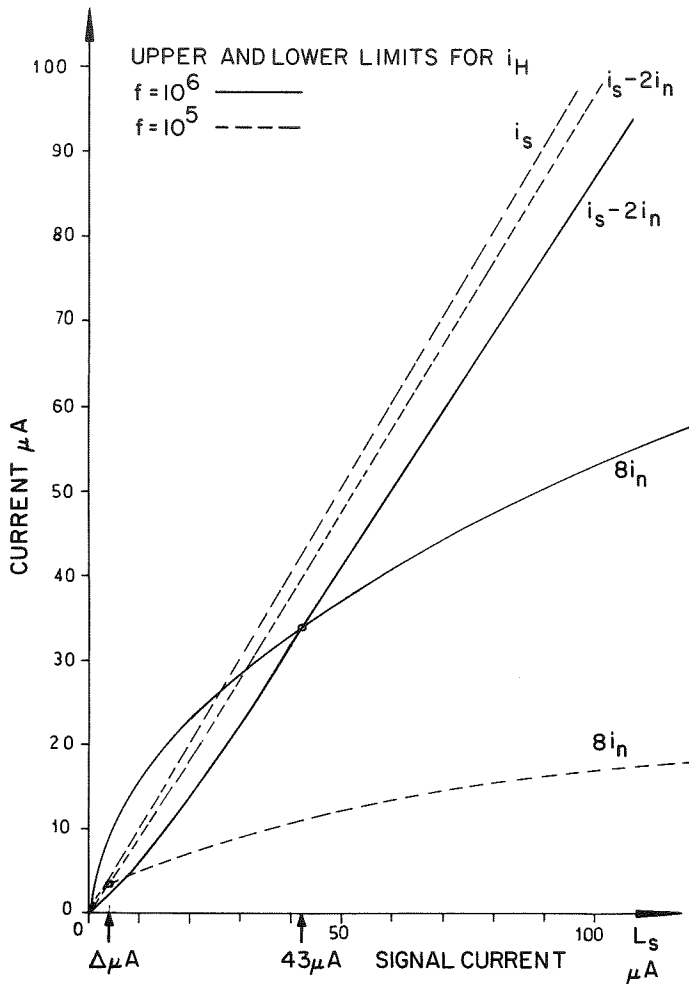


Fig. 6. Noise boundaries to the values of the hysteresis current of the discriminators.

contribution has been minimized, the random fluctuations still contribute a variance  $F\sqrt{\tau_2 T}$ , which has to be compared with the number of counts  $L = d/(\lambda/8)$  associated with the path difference  $d$ , in order to yield a relative precision of the measurement. For instance, if  $d = 100$  m,  $\tau_2 = 10^{-5}$  sec,  $F = 3 \cdot 10^2$  sec $^{-1}$  and we want a precision better than  $10^{-8}$ , the maximum observation time is  $T = 100$  sec.

#### ACKNOWLEDGMENT

We wish to thank Prof. E. Gatti for helpful discussions during this work.

## REFERENCES

1. F. T. Arecchi and A. Sona, *Nuovo Cimento*, Vol. 32, p. 1117 (1964).
2. T. Morokuma, K. F. Neflen, T. R. Lawrence and T. M. Klucher, *J. Opt. Soc. Am.*, Vol. 53, p. 394 (1963).
3. R. Grundzinski and M. Paillette, *Compt. Rend. Acad. Sci.*, Vol. 257, p. 3842 (1963).
4. T. S. Jaseja, A. Javan and C. H. Townes, *Phys. Rev. Lett.*, Vol. 10, p. 165 (1963).
5. D. A. Kleinman and P. P. Kisliuk, *Bell Syst. Tech. J.*, Vol. 41, p. 453 (1962).
6. H. Kogelnik and C. K. N. Patel, *Proc. I.R.E.*, Vol. 50, p. 2365 (1962).
7. E. R. Peck and S. W. Obetz, *J. Opt. Soc. Am.*, Vol. 43, p. 505 (1953).
8. F. T. Arecchi, G. Lepre and A. Sona, "A New Reversible High Speed Fringe Counter for Laser Interferometry" (to be published in *Alta Frequenza*).
9. A. Consortini, L. Ronchi, A. M. Scheggi and G. Toraldo di Francia, *Alta Frequenza*, Vol. 32, p. 790 (1963).
10. G. Toraldo, et al., "Influence of Atmospheric Scattering on the Line-Width of a Laser Beam" (to be published in *Alta Frequenza*).